Research article

Benjamin Gallinet*, Giorgio Quaranta and Christian Schneider

Narrowband transmission filters based on resonant waveguide gratings and conformal dielectric-plasmonic coatings

https://doi.org/10.1515/aot-2020-0049
Received August 11, 2020; accepted October 13, 2020;
published online November 2, 2020

Abstract: Nanostructured filter arrays on image sensors are promising for miniature spectrometers and spectral imagers. In this work, we report on resonant waveguide gratings fabricated by UV nanoimprint lithography and conformal dielectric-plasmonic coatings. Optical measurements in accordance with numerical simulations report on a resonance bandwidth of 20 nm in transmission in the visible range. The impact of cladding thickness and filter lateral size on the resonance properties is investigated with the help of numerical calculations. Finally, it is shown that the proposed geometry based on conformal coatings has a very efficient blocking rate compared to other nanostructured filter approaches.

Keywords: guided mode resonances; plasmon; resonant waveguide gratings; transmission filter; UV nanoimprint.

There has been recently an increasing interest in miniature devices performing spectral measurements for a variety of applications such as photography or food analysis in consumer electronics, as well as human centric lighting or industrial quality control (see e.g. the studies by Liu et al., Kha et al. and Goldring et al. [1–3]). Compact spectral sensors, spectrometers and spectral imagers are ideally manufactured as a filter array on image sensors (see e.g. the study by Geelen et al. [4]). This need is also associated with constraints on the efficiency of the fabrication process and ease of integration. When considering interference filters for example, their spectral positions depend on thicknesses of the applied coatings. As the number of required spectral bands increases, the number of filters and resulting number of process steps is expected to increase. Nanostructured filters have been identified in this context as potential candidates to overcome these constraints, as they can be manufactured with a low amount of process steps which does not scale with the number of spectral channels. The wavelength range that they are addressing is related only to some design parameters, such as the pitch or fill factor of the resonant structures. Among them, plasmonic array naturally has a resonant response in transmission and has been demonstrated in miniature spectrometers, as RGB filter arrays on CMOS image sensors [5] or as spectral sensors [6, 7]. They are however limited by optical losses from metallic absorption, especially in the visible and near infrared ranges, which prevents accessing to smaller spectral bandwidths. On the other hand, resonant waveguide gratings, also known as guide mode resonant devices, are based on high refractive index dielectric materials and thus can offer access to spectrally narrower resonances [8]. Photonic crystals have also been shown to support guided mode resonances [9]. Different approaches using a guided mode resonance in combination with surface plasmon resonance to generate bandpass filters have been proposed [10, 11], with bandwidths down to 20 nm [10, 12]. In the study by Wang et al. [13], hybrid plasmonic and resonant waveguide structures have been used as free-standing membranes to generate RGB filters with high transmission. These approaches rely on the use of a flat waveguide and etching of thin metallic films, which implies some constraints on manufacturing.

In this work, we report on narrowband hybrid filters fabricated by UV nanoimprint lithography and conformal coatings. We show that the distribution of refractive index induced by the thin films deposited on the corrugated surface effectively generates a waveguide core, cladding and metallic grid. Using this method, transmission peaks with FWHM of 20 nm and a low nonresonant background contribution are measured. We analyze the impact of the different structure parameters on the resonance properties,

***Corresponding author: Benjamin Gallinet**, CSEM Muttenz, Tramstrasse 99, 4132 Muttenz, Switzerland,
E-mail: benjamin.gallinet@csem.ch. https://orcid.org/0000-0001-7444-3398
Giorgio Quaranta and Christian Schneider, CSEM Muttenz, Tramstrasse 99, 4132 Muttenz, Switzerland

in particular the upper and lower cladding thicknesses, the filter lateral dimensions. We compare the presented approach of conformal coatings to approaches resulting in planar geometries and quantitatively show how the conformal coatings have better filtering performances, especially when a large spectrum extending over visible and near-infrared is considered. The fabrication method is compatible with large throughput in manufacturing.

Our filters are composed of a periodically corrugated resonant waveguide grating, on top of which sits an array of corrugated plasmonic nanowires. Despite the corrugation, a cladding and a core layer can be defined by considering the average refractive index of the different dielectric layers. Figure 1a summarizes the incoupling, outcoupling and Fano interference processes building the filtering effect. The incident light is coupled by the periodic structure into propagating surface plasmons at metal–dielectric interfaces. Surface plasmons are then funneled through the small apertures and coupled into the dielectric waveguide. The waveguide mode is finally outcoupled by the periodic structure to the substrate. A more detailed account on the coupling mechanisms between the waveguide and the metallic wires can be found in the study by Bauer and Giessen[14]. At resonance, the Fano interference between the light outcoupled from the waveguide and the continuum of the directly transmitted light yield in a transmission peak, in a similar way to the extraordinary transmission effect in plasmonic aperture arrays [15, 16]. The Fano effect can be here understood as an interference between the in- and outcoupled optical field (black arrows in Figure 1a) and the continuum of directly reflected and transmitted light (red arrows in Figure 1a). Around the resonance wavelength, the in- and outcoupled field undergoes a phase shift, which results either in constructive or destructive interference with the continuum. Since the off-resonant transmission is low, the constructive interference at resonance in transmission is dominant, thus resulting in a transmission peak (Figure 1b).

A dielectric low index spacer is present between the plasmonic nanostructures and the waveguide in order to limit optical losses. In order to maximize the resonance amplitude, the dielectric spacer (i.e., the upper cladding) and the lower cladding must be of similar refractive index. SiO_2 has been chosen as the spacer material and thus matches the refractive index of the underlying UV curable resin. The core material should have the highest contrast possible with the cladding. We have chosen ZnS with an index of approximately 2.3 for this study. Regarding the choice of the plasmonic material, aluminum and silver are widespread for resonances in the visible range, including

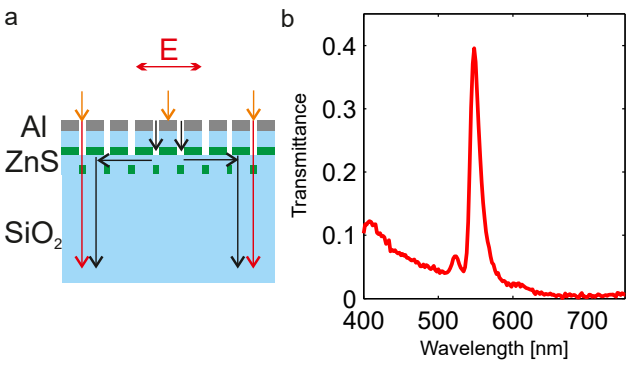

Figure 1: (a) Light propagation in the proposed hybrid plasmonic dielectric corrugated waveguide system. The incident light (orange arrows) is coupled by plasmonic resonances in the metallic top coating, into a resonant waveguide grating made of a ZnS core (green) conformal to a periodic corrugation, and finally coupled out (black arrows). It interferes with directly transmitted light (red arrows) to form a Fano-like resonance. A silica spacer (blue) is present between the metallic layer and the waveguide core.
(b) Measured transmittance spectrum of TM-polarized light.

the lower wavelengths. Since silver shows a large plasmonic contribution in the transmission outside of the guided mode resonances, aluminum has been preferred.

The background of directly transmitted light is relatively low due to the small gap between aluminum nanowires. The ratio of background amplitude to peak amplitude typically ranges between –20 and –6 dB for TM polarization (electric field perpendicular to the grating lines), and generally below –12 dB for TE polarization (which is featureless, not shown here). In the present case, the in-plane propagating modes are supported by the dielectric waveguide instead of the plasmonic structures, which results in reduced optical losses and a higher mode quality factor. The measured transmittance spectra for TM polarization show a bandwidth of 20 nm at a wavelength of 550 nm (Figure 1b).

The fabrication process flow is shown in Figure 2a–e. A master consisting of a binary profile is generated by electron beam lithography and etching in a silicon wafer. A nanoimprint master is fabricated from the silicon wafer, which is used to replicate the nanostructure in a UV curable material. The profile of the master has a corrugation depth of 80 nm in order to compensate for the profile loss during the replication step (typically in the order of 10%). Ten different periods have been investigated in this work in order to cover homogeneously the visible range, namely 260, 288, 316, 344, 372, 400, 428, 456, 484 and 512 nm. The corrugation depth d = 70 nm, the spacing between grating lines w = 100 nm, the ZnS thickness t_w = 50 nm, the SiO_2 spacer thickness t_c = 80 nm and the aluminum thickness

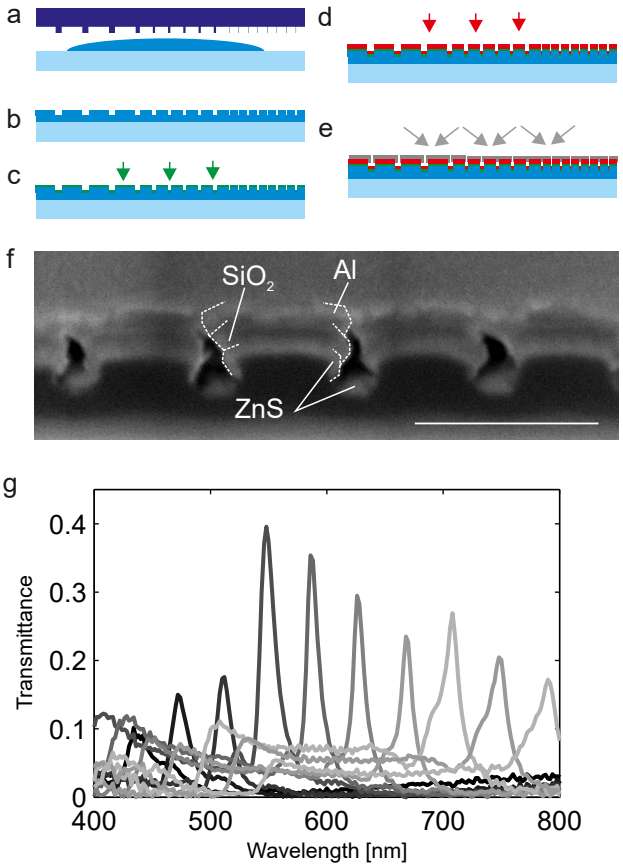

Figure 2: (a–e) Fabrication process flow. (a) UV nanoimprint lithography from a master containing 10 different linear binary grating profiles. (b) Transferred grating profiles in UV curable material on transparent substrate (dark blue). (c) Coating of waveguide core material (ZnS, green arrows). (d) Coating of cladding and spacer material (SiO_2, red arrows) (d) Oblique aluminum metallization (gray arrows). (f) Scanning electron micrograph of fabricated nanostructure. Scale bar: 400 nm. (g) Measurement of corresponding transmittance for TM-polarized light. From left to right: periodicity of the corrugation of 260, 288, 316, 344, 372, 400, 428, 456, 484 and 512 nm. The coatings are applied simultaneously to all gratings.

$t_m = 40$ nm evaporated with an angle of 60° from the normal of the substrate to ensure a deposition only on the top of the grating. In order to show the potential of this approach to effectively generate filter arrays, these 10 different gratings have been processed simultaneously on the same substrate. Due to manufacturing constraints the corrugation depth must be comparable to $t_w + t_m$, so that the ZnS and SiO_2 films deposition does not alter the profile before the Al coating. Using this approach, an array of metallic apertures supporting propagating surface plasmons is generated [17]. A cross section of the fabricated structured has been performed with focused ion beam milling and analyzed with a scanning electron microscope (Figure 2f). It can be observed that the aluminum coating is almost closed but that a gap between individual elements remains, which allows coupling to the underlying waveguide. Measurements and simulations of completely closed gaps (not shown here) show a nonresonant and very low transmission level, thus confirming that an opening in the metallic layer, even small, must be present for surface plasmons to funnel through. Figure 2g shows the corresponding transmission measurement for the various filter devices. For all of them, the FWHM of the transmission peak is around 20 nm, while the peak transmission ranges between 10 and 40%.

In the following, we analyze the different effects impacting the resonance amplitude with support of numerical simulations. The simulation of the filters has been performed with the rigorous coupled wave analysis (RCWA), with 40 diffraction orders in the Fourier decomposition of the field in order to account for numerical inaccuracies in TM polarization [18]. The geometry considered for a given filter is sketched in Figure 3a, while the simulations results for all filters are reported in Figure 3b. The corrugation depth $d = 70$ nm, the spacing between grating lines $w = 100$ nm, the ZnS thickness $t_w = 50$ nm, the SiO_2 spacer thicknesses $t_c = 80$ nm and $t'_c = 30$ nm, the aluminum thickness $t_m = 40$ nm, the sidewall thickness $w_s = 40$ nm and the top metal width $w_m = p - w + w_s$. The peak positions, FWHM and amplitude of background transmission are in very good agreement with measurements. However, numerical calculations appear to overestimate the peak amplitude. First, the measurement beam divergence is approximately 1°. Thus, simulations have been performed for 1° incidence from the normal of the plane, in the direction across the grating lines (Figure 3c). Comparing Figure 3b and Figure 3c, simulations predict a difference of 10–40% in peak transmission amplitude for a deviation of 1° in beam incidence from the surface normal, depending on the filter geometry. At normal incidence, the first and minus first orders are coupled at the same wavelength in the waveguide and their contributions directly add up in the total resonance intensity. A non-normal incidence results in a difference in excitation wavelengths of these two modes and as a result a splitting of their resonances and a reduction of the peak transmission. The larger and shorter wavelengths are also more sensitive to the incidence angle, because the waveguide core thickness is chosen to optimize the central wavelengths. This result in a peak amplitude in simulation ranging between 20 and 60%. Still, the simulated peak amplitude is larger than measured, which is attributed to structural variations within the measurement spot (with a diameter of approximately 2 mm). This has the effect of

introducing a so-called inhomogeneous broadening in the resonance. In weakly coupled Fano-resonant systems, it results in affecting mostly the resonant amplitude as the interference between the in and out-coupled field and the continuum is damped [19]. Since the number of grating periods contributing to the measurement is very large and geometrical variations are expected, homogeneous broadening is expected to play an important role in the decrease of the resonance amplitude from simulations. Figure 3d shows the same simulation as Figure 3b but with silver instead of aluminum. It can be seen that strong localized surface plasmon resonances prevent an efficient blocking outside of the guided mode resonance.

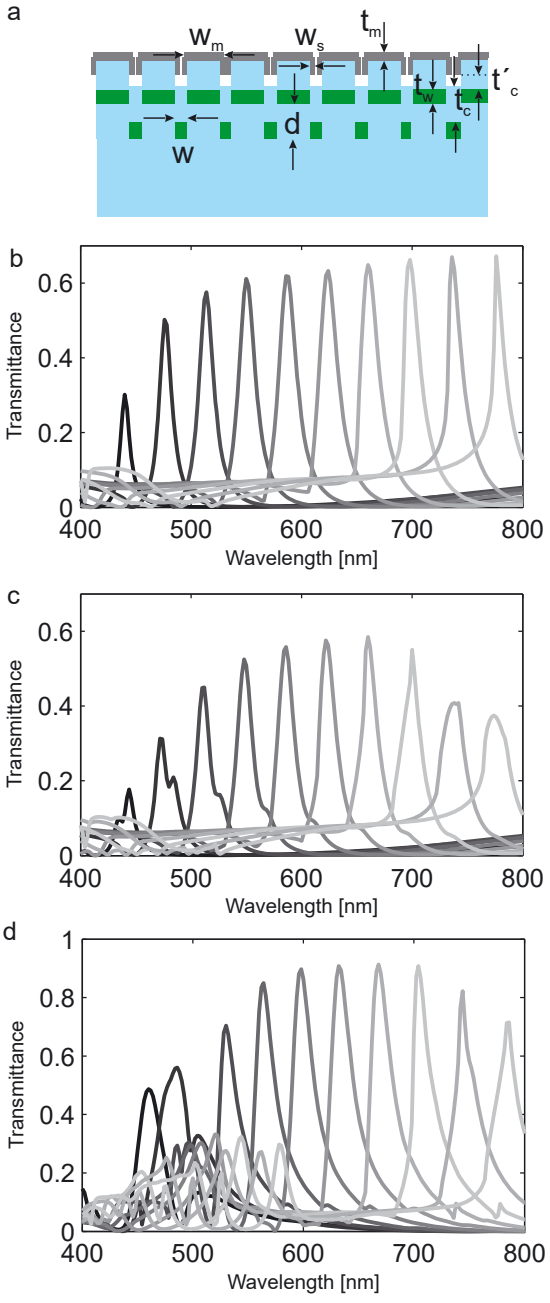

Figure 3: Numerical simulation of filter transmission using rigorous coupled wave analysis (RCWA). (a) Schematic of simulated geometry and parameters definition. (b) Transmission at normal incidence for TM polarization. (c) Transmission at 1° from normal incidence for TM polarization. (d) Transmission at normal incidence with silver in place of aluminum. From left to right: periodicity of the corrugation of 260, 288, 316, 344, 372, 400, 428, 456, 484 and 512 nm.

The upper and lower dielectric layers of the waveguide strongly influence the resonance amplitude and position, as illustrated in Figure 4. The low index dielectric spacer between the metallic nanowires and the waveguide plays the role of cladding and its thickness influences the coupling strength between surface plasmons supported by the metallic nanowires and the dielectric waveguide modes. For a low spacer thickness, the propagating modes have a strong contribution from the surfaces plasmons, optical losses are higher and the mode FWHM is in the range of 30 nm (Figure 4b). When the thickness is increased to higher values, surface plasmons do not efficiently couple evanescently to the dielectric waveguide modes and the peak amplitude is reduced. The optimal spacer thickness is therefore in the range of 80–100 nm. In addition, the lower cladding plays an important role in the resonance properties, which is relevant for applications where the filter is constructed for example as a membrane or directly integrated on a semiconductor for light harvesting. In the simulations of Figure 4c, the material under the waveguide is air and a cladding of SiO_2 under the waveguide is considered. When the waveguide is directly in contact with air, the mode propagation is pulled on the upper side of the waveguide and affected by optical losses from the metallic nanowires [10]. When the thickness of the lower cladding is comparable to the effective wavelength in SiO_2, additional modes arising from total internal reflections at the lower dielectric-to-air interface appear, with a signature of multiple peaks. The spectral spacing between the modes is reduced as t_B is increased. For a very thick lower spacer, the resonance wavelength of higher-order modes converges to the wavelength of the fundamental mode. Depending on the source coherence, the higher-order modes can be suppressed for large spacer thickness. Figure 4d shows a similar study for a silicon substrate, representing for example the filter directly integrated onto an image sensor. The imaginary part of the permittivity of silicon has been set to zero in order to compute the transmitted intensity in the far-field. It can be observed that a lower cladding layer of 500 nm of SiO_2 is required to reach a similar performance level to the case without silicon (t_B = infinity). The FHWM is also slightly increased in this case. The higher the cladding thickness,

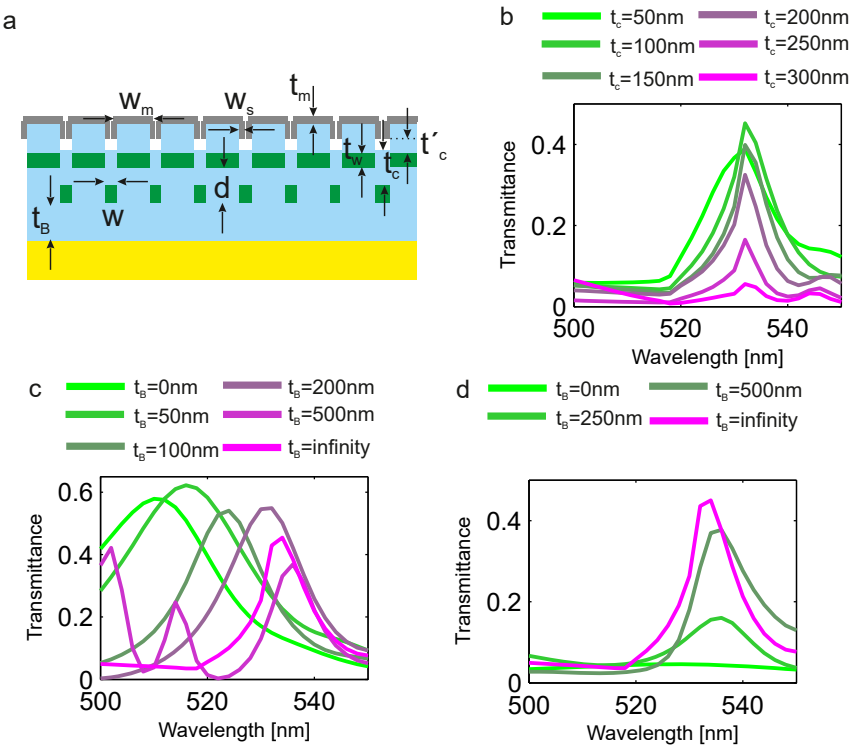

Figure 4: Influence of upper and lower claddings on resonance properties. (a) A lower cladding of SiO_2 of thickness t_B is inserted between the waveguide and substrate. (b) Simulated filter transmission as a function of upper cladding thickness t_B for period 344 nm, waveguide thickness t_w = 35 nm and infinite lower cladding thickness (b–c) Simulated filter transmission as a function of lower cladding thickness t_B for an (b) air and (c) silicon substrate and t_C = 80 nm.

the lower optical losses from silicon absorption are expected.

Finite differences in time domain (FDTD) simulations have been performed in order to estimate the minimal filter dimension required to support the resonance. Compared to RCWA, FDTD allows in a straightforward manner simulation of finite sized systems, with perfectly matched layers (PMLs) at boundaries of the computation window. Figure 5a shows the near-field intensity distribution at resonances (wavelength 600 nm) for the 372 nm grating, with a total lateral dimension of 30 µm in the direction across the grating lines. As they are two-dimensional calculations, the grating extends infinitely in the direction along the grating line, but it is expected to have a low impact in this direction. The mode field extends below the waveguide up to approximately 400 nm, which confirms the findings from Figure 4b and c that the resonance is affected by changes in the substrate material in this region. The beam diameter is kept constant at 20 µm, as it is shown to have an influence on the grating resonance amplitude and wavelength [20, 21]. The detectors size, i.e., the zone where the field amplitude is sampled, is 2 µm. One can directly observe the signature of a guided mode resonance in the ZnS layer below, as well as surface plasmon resonance in the gap between the aluminum structure. For the direction across the grating lines, Figure 5b reports the peak amplitude as a function of the grating lateral extension. At 15 µm and above, the peak amplitude is relatively comparable, which gives an estimation of the minimal lateral size required in order to have a full resonance. Below 15 µm, the resonance is still present, but with less amplitude. In the measurements of Figure 1 and Figure 2, the gratings have lateral dimensions of 3 mm and the measurement beam diameter is approximately 2 mm, thus excluding any finite-size effect.

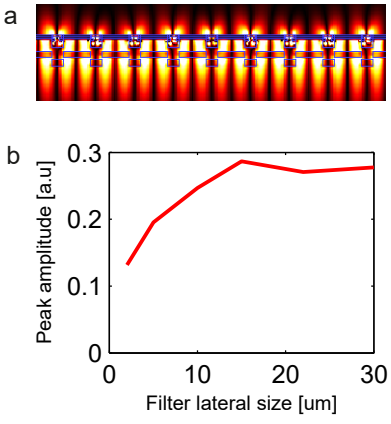

Figure 5: Finite differences in time domain (FDTD) simulation of filters with finite lateral size. (a) Numerical simulation of TM-polarized electric field intensity at wavelength 600 nm for the 372 nm period filter. (b) Calculation of resonance peak intensity at 600 nm for a filter as function of its lateral size.

A bandpass optical filter must have the ability to efficiently block the wavelengths outside of its transmission band, which will determine the signal to noise ratio and resulting performance in spectrometric and spectral imaging applications. We now would like to analyze how the proposed approach based on conformal coatings impacts the optical blocking, especially in comparison with previously established geometries based on planar metallic nanowires and dielectric layers [10–12]. In order to obtain a planar geometry with resonance wavelength, FWHM and peak transmission comparable to the conformal coating geometry, the effective core and cladding refractive index have been calculated by averaging the contributions from the ZnS, SiO_2 and air materials, as illustrated in Figure 6a. The effective core thickness t'_w is 120 nm, the effective cladding thickness t'_c is 100 nm. For the metallic layer parameters, we have $t'_m = t_m$ and $w'_m = w_m$. Comparing Figure 6b to Figure 3c, we observe a large broadband off-resonance transmission at large wavelengths, especially for filters resonant in the low wavelength range. This effect is observed also experimentally [10–12] and can be interpreted as follows: in the case of conformal coatings, metallic sidewalls are able to funnel surface plasmons at resonance and couple them into the waveguide, while they will further reduce off-resonance transmission at large wavelengths by bringing additional amount of bulk metallic material. The difference between conformal coatings and planar metallic wires is even larger in the near-infrared (spectra not shown here).

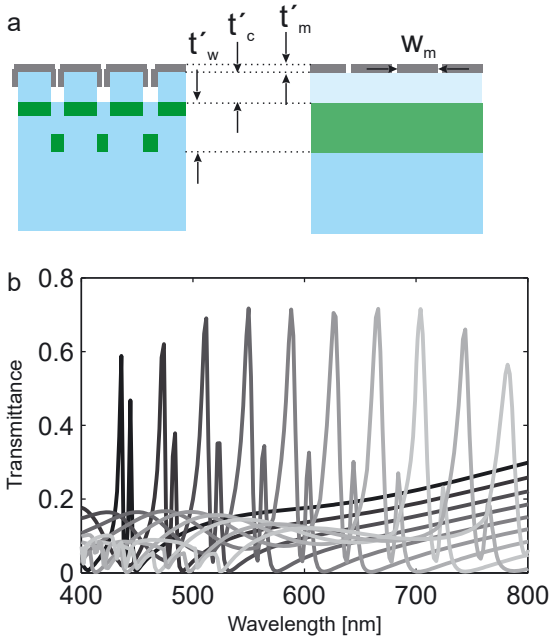

Figure 6: Numerical simulation of filter transmission reproduced with an effective planar waveguide geometry. (a) Schematic of simulated geometry and parameters definition. (b) Transmission at 1° from normal incidence for TM polarization. From left to right: periodicity of the corrugation of 260, 288, 316, 344, 372, 400, 428, 456, 484 and 512 nm.

In order to quantitatively assess the difference in optical blocking between the conformal and planar nanowires, we define the filter weight F as follows:

$$F = \frac{\int_{\lambda_0-\Delta\lambda/2}^{\lambda_0+\Delta\lambda/2} T(\lambda)d\lambda}{\int_{\lambda_{min}}^{\lambda_{max}} T(\lambda)d\lambda}, \quad (1)$$

which corresponds to the fraction of transmitted intensity over the filter bandwidth $\Delta\lambda$ centered on λ_0, to the transmitted intensity over the total spectral range between λ_{min} and λ_{max}. Here the filter bandwidth is defined as $\Delta\lambda = 2$ FWHM = 40 nm consistently for all filters. Figure 7a shows how the filter bandwidth is selected. The calculation of filter weight F is performed from simulated and measured transmission spectra for the conformal coating approach, and from simulated spectra of the planar filters approach. The wavelength range is chosen in Figure 7b to be $\lambda_{min} = 380$ nm and $\lambda_{max} = 800$ nm. Several observations can be made: first the conformal coatings clearly outperform planar nanowires for most grating periodicities, especially the short periods where the resonance wavelength is low. Second, the incidence angle does not really impact this result, although the peak transmission is lower for 1° incidence. Figure 7c extends the wavelength range to $\lambda_{max} = 1080$ nm corresponding approximately to the end of the silicon absorption band. The difference between planar and conformal metallic nanowires is even larger for all grating periodicities, with up to a 10 × larger filter weight for conformal metallic nanowires. Therefore, although the filters presented here have a lower peak transmission level than approaches based on planar nanowires, their blocking is in general multiple times more efficient. We also stress that this trend on the filter weight is independent of the metal thickness, as both peak transmission and blocking rate depends on the metal thickness.

In conclusion, this article has reported on filter arrays based on hybrid resonant waveguide and plasmonic nanostructures. Their fabrication using UV nanoimprint lithography and conformal coatings prevent the use of etching and lift-off steps, which makes it a promising approach for upscaled manufacturing with high throughput. A FWHM of 20 nm in transmission is reported, with filter central wavelengths ranging between 420 and 800 nm. Numerical simulations show a good agreement with measurements for the transmission peak wavelength, the FWHM and background transmission. We have then investigated the impact of cladding on the resonance

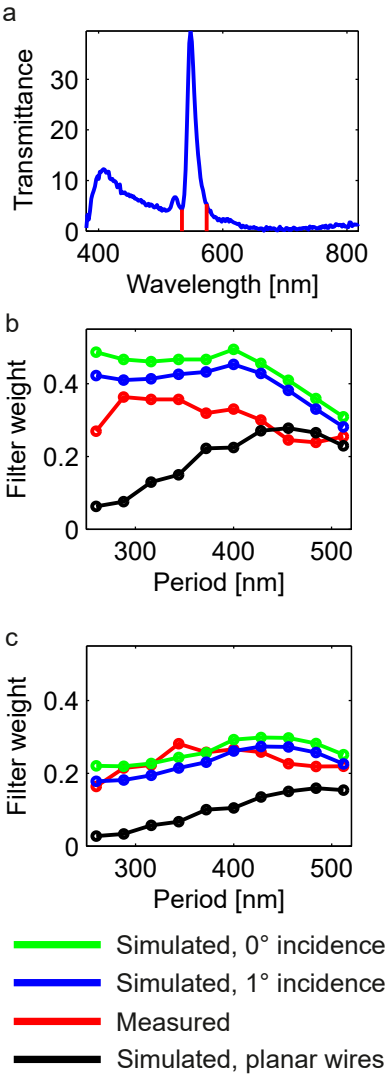

Figure 7: Calculation of filter weight according to Equation (1). (a) Selection of filter bandwidth of 40 nm around the resonance wavelength. (b) Filter weight F considering a total spectrum from 380 to 800 nm. (c) Filter weight considering a total spectrum from 380 to 1080 nm.

properties. In particular, there is an optimal spacer thickness between the metallic and waveguide layers, and the waveguide layer must be placed on top of a cladding layer too keep narrowband operation. Further investigations with FDTD show that the filter should have a minimal size of approximately 15 µm in order to have a full resonance. Finally, we have shown that a geometry based on conformal coatings compared to flat metallic nanowires is able to block significantly better wavelengths outside the transmission band, which is extremely relevant for spectrometric and spectral imaging applications. This difference is increased when the visible and near-infrared range is considered. The presented approach can be applied to the NIR and SWIR ranges with adaptation of the structure parameters. Alternative high refractive index materials such as aluminum, tantalum, niobium or titanium oxides can be used as waveguide. The fabrication process of UV nanoimprint is also applicable directly on image sensors, in a similar way to e.g. microlens arrays [22], over single or multiple pixels depending on the individual pixel size. Overall, the presented filter approach is foreseen to find applications in compact and mass manufactured miniature spectral sensors and multispectral cameras.

Author contribution: All the authors have accepted responsibility for the entire content of this submitted manuscript and approved submission.
Research funding: None declared.
Conflict of interest statement: The authors declare no conflicts of interest regarding this article.

References

[1] Y. Liu, H. Pu, and D.-W. Sun, "Hyperspectral imaging technique for evaluating food quality and safety during various processes: A review of recent applications," *Trends Food Sci. Technol.*, vol. 69, pp. 25–35, 2017.
[2] M. J. Khan, H. S. Khan, A. Yousaf, K. Khurshid, and A. Abbas, "Modern trends in hyperspectral image analysis: a review," *IEEE Access*, vol. 6, pp. 14118–14129, 2018.
[3] D. Goldring, D. Sharon, S. Rosen, et al., "Spectrometry system with visible aiming beam," WO Patent 2016/125165, Aug. 11, 2016.
[4] B. Geelen, A. Lambrechts, and K. Tack, "Spectral camera with mosaic of filters for each image pixel," US Patent 9857222, Jan. 2, 2018.
[5] S. Yokogawa, S. P. Burgos, and H. A. Atwater, "Plasmonic color filters for CMOS image sensor applications," *Nano Lett.*, vol. 12, pp. 4349–4354, 2012.
[6] S. Junger, W. Tschekalinskij, and N. Weber, "Optical bandpass filter system, in particular for multichannel spectral-selective measurements," WO Patent 2012/007147, Jul. 11, 2011.
[7] B. I. Choi, B. Lee, and M. K. song, "Nano-optic filter array based sensor," US Patent 2012/0129269, May 24 2012.
[8] G. Quaranta, G. Basset, O. J. F. Martin, and B. Gallinet, "Recent advances in resonant waveguide gratings," *Laser Photonics Rev.*, vol. 12, p. 1800017, 2018.
[9] S. Fan and J. D. Joannopoulos, "Analysis of guided resonances in photonic crystal slabs," *Phys. Rev. B*, vol. 65, p. 235112, 2002.
[10] A. F. Kaplan, T. Xu, and L. J. Guo, "High efficiency resonance-based spectrum filters with tunable transmission bandwidth fabricated using nanoimprint lithography," *Appl. Phys. Lett.*, vol. 99, p. 143111, 2011.
[11] Y.-T. Yoon, C.-H. Park, and S.-S. Lee, "Highly efficient color filter incorporating a thin metal–dielectric resonant structure," *Appl. Phy. Express*, vol. 5, p. 022501, 2012.
[12] D. B. Mazulquim, K. J. Lee, J. W. Yoon, et al., "Efficient band-pass color filters enabled by resonant modes and plasmons near the Rayleigh anomaly," *Opt. Express*, vol. 22, p. 30843, 2014.

[13] J. Wang, Q. Fan, S. Zhang, et al., "Ultra-thin plasmonic color filters incorporating free-standing resonant membrane waveguides with high transmission efficiency," *Appl. Phys. Lett.*, vol. 110, p.031110, 2017.

[14] C. Bauer and H. Giessen, "Tailoring the plasmonic Fano resonance in metallic photonic crystals," *Nanophotonics*, vol. 9, pp. 523–531, 2020.

[15] C. Genet, M. P. van Exter, and J. P. Woerdmann, "Fano-type interpretation of red shifts and red tails in hole array transmission spectra," *Opt. Commun.*, vol. 225, pp. 331–336, 2003.

[16] M. Sarrazin, J.-P. Vigneron, and J.-M. Vigoureux, "Role of Wood anomalies in optical properties of thin metallic films with a bidimensional array of subwavelength holes," *Phys. Rev. B*, vol. 67, p.085415, 2003.

[17] F. Lütolf, O. J. F. Martin, and B. Gallinet, "Fano-resonant aluminum and gold nanostructures created with a tunable, up-scalable process," *Nanoscale*, vol. 7, p. 18179, 2015.

[18] P. Lalanne and G. M. Morris, "Highly improved convergence of the coupled-wave method for TM polarization," *J. Opt. Soc. Am. A*, vol. 13, pp. 779–784, 1996.

[19] B. Gallinet, T. Siegfried, H. Sigg, P. Nordlander, and O. J. F. Martin, "Plasmonic radiance: Probing structure at the ngström scale with visible light," *Nano Lett.*, vol. 13, pp. 497–503, 2013.

[20] J. M. Bendickson, E. N. Glytsis, T. K. Gaylord, and D. L. Brundrett, "Guided-mode resonant subwavelength gratings: effects of finite beams and finite gratings," *J. Opt. Soc. Am. A*, vol. 18, pp. 1912–1928, 2001.

[21] G. Niederer, H. P. Herzig, J. Shamir, H. Thiele, M. Schnieper, and C. Zschokke, "Tunable, oblique incidence resonant grating filter for telecommunications," *Appl. Opt.*, vol. 43, pp. 1683–1694, 2004.

[22] I. Gyongy, A. Davies, B. Gallinet, et al., "Cylindrical microlensing for enhanced collection efficiency of small pixel SPAD arrays in single-molecule localisation microscopy," *Opt. Express*, vol. 26, pp. 2280–2291, 2018.